ChemComm

COMMUNICATION

View Article Online
View Journal | View Issue

Cite this: *Chem. Commun.*, 2017, 53, 6164

Received 14th March 2017,
Accepted 15th May 2017

DOI: 10.1039/c7cc01845b

rsc.li/chemcomm

Dielectrophoretic assembly of liquid-phase-exfoliated TiS_3 nanoribbons for photodetecting applications†

R. Frisenda, *[a] E. Giovanelli, [a] P. Mishra,[a] P. Gant,[a] E. Flores,[b] C. Sánchez, [b] J. R. Ares,[b] D. Perez de Lara,[a] I. J. Ferrer, [b] E. M. Pérez *[a] and A. Castellanos-Gomez ‡*[a]

Liquid-phase exfoliation is a technique capable of producing large quantities of two-dimensional materials in suspension. Despite many efforts in the optimization of the exfoliation process itself, not much has been done towards the integration of liquid-phase-exfoliated materials in working solid-state devices. In this article, we use dielectrophoresis to direct the assembly of liquid-phase-exfoliated TiS_3 nanoribbons between two gold electrodes to produce photodetectors working in the visible region. Through electrical and optical measurements we characterize the responsivity of the device and we find values as large as 3.8 mA W^{-1}, which are more than one order of magnitude higher compared to state-of-the-art devices based on liquid-phase-exfoliated two-dimensional materials assembled by drop-casting or ink-jet methods.

Right after the first works on mechanically exfoliated two-dimensional (2D) materials,[1–3] other preparation methods oriented toward their larger scale production have been rapidly explored and developed. A significant example of a bottom-up approach is chemical vapor deposition (CVD) that provides a way to synthesize high quantities of homogenous materials with large crystalline domains,[4–6] but is costly and complicated. From the top-down perspective, liquid-phase exfoliation (LPE) is an appealing route to produce large amounts of 2D materials in the form of small crystallites suspended in a solvent.[7–13] LPE represents a cheap technique that can be easily scaled up and has strong potential to be used in printed electronics.

Significant efforts have been made in the optimization of the LPE process,[14–19] mostly aimed at controlling the thickness and lateral size of the flakes and increasing the concentration of the suspensions. However, the integration of LPE materials into functional devices still remains largely unexplored, with the exception of devices based on graphene inks.[20,21] Additionally, Withers *et al.*[22] showed that heterostructures could be assembled from liquid-phase-exfoliated 2D crystals and they designed a photodetector with a gate-tunable photoresponsivity of up to 43 μA W^{-1}. In a different study, Yang *et al.*[23] incorporated liquid-phase-exfoliated materials as dielectrics in graphene-based photodetectors. Zhu *et al.*[24] reported similar findings on the outstanding dielectric properties of liquid inks made from thickness-sorted 2D hexagonal boron nitride.

Here, we demonstrate how titanium trisulfide (TiS_3) nanoribbons obtained by LPE can be assembled between two metallic electrodes by dielectrophoresis (DEP) to fabricate photodetectors. TiS_3 is a layered material that belongs to the family of semiconducting transition metal trichalcogenides and exhibits pronounced in-plane anisotropy[25] and great potential to be used in optoelectronics.[26–28] In the present paper we use DEP-assisted deposition to assemble liquid-phase-exfoliated TiS_3 nanoribbons in between metallic electrodes to produce solid-state photodetectors. The device based on colloidal TiS_3 shows improved responsivities as large as 3.8 mA W^{-1} compared to state-of-the-art LPE-based devices. The novel deposition method based on DEP, together with the excellent photodetecting properties of TiS_3 retained in the liquid-phase-exfoliated material, paves the way for fabrication of novel and cheap photodetectors which can be easily scaled up for industrial applications.

Bulk TiS_3 was prepared by surface sulfurization of bulk Ti powder at 500 °C, similarly to the procedure described in ref. 29. Fig. 1a shows a scanning electron microscopy (SEM) picture of lamellar bulk TiS_3 and in the inset a photograph of the as-synthetized bulk TiS_3 (Fig. S1, ESI†). We prepared TiS_3 suspensions by ultrasonication of the bulk material in isopropyl alcohol (IPA). We employed successive centrifugation–redispersion sequences to sort out the suspensions according to TiS_3 crystallite dimensions. Fig. 1b shows a photograph of four suspensions of TiS_3 in IPA. From suspension A, resulting directly from the sonication step, three other suspensions labelled B, C and D

[a] *Instituto Madrileño de Estudios Avanzados en Nanociencia (IMDEA-Nanociencia), Campus de Cantoblanco, E-28049 Madrid, Spain. E-mail: riccardo.frisenda@imdea.org, emilio.perez@imdea.org, andres.castellanos@csic.es*

[b] *Materials of Interest in Renewable Energies Group (MIRE Group), Dpto. de Física de Materiales, Universidad Autónoma de Madrid, 28049 Madrid, Spain*

† Electronic supplementary information (ESI) available. See DOI: 10.1039/c7cc01845b

‡ Present address: Instituto de Ciencia de Materiales de Madrid (ICMM-CSIC), Campus de Cantoblanco, E-28049 Madrid, Spain.

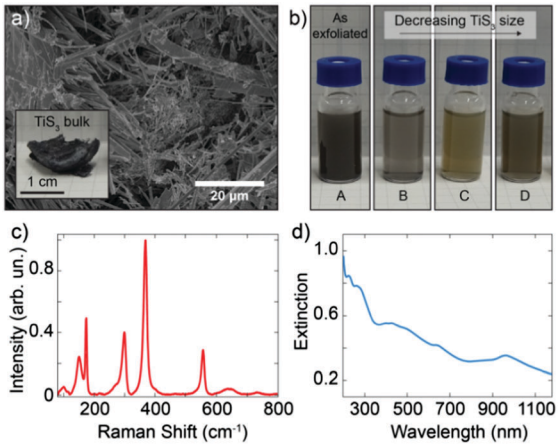

Fig. 1 (a) SEM image of the lamellar TiS_3 bulk material. Inset: Photograph of bulk TiS_3. (b) Optical image of the colloidal suspensions of exfoliated TiS_3 in IPA. (c) Raman spectrum (normalized at 368 cm^{-1}) and (d) UV-Vis-NIR spectrum of colloidal suspension D.

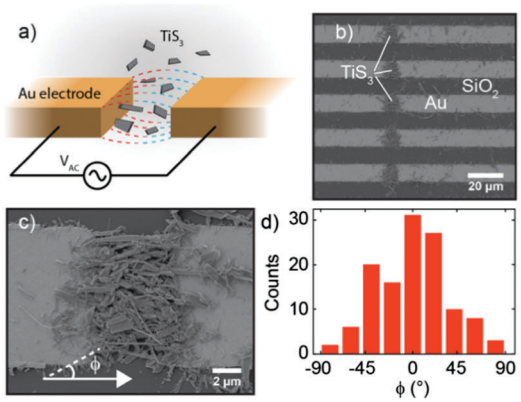

Fig. 2 (a) Sketch of the DEP technique used to fabricate TiS_3-based photodetecting devices from the liquid-phase-exfoliated material. (b and c) SEM images of aligned TiS_3 nanoribbons between gold electrodes assembled from suspension D. (d) Angular distribution of the assembled TiS_3 nanoribbons where 0° corresponds to a nanoribbon oriented along the source–drain electrode direction. The angle was measured from 123 nanoribbons identified in the SEM image of panel (c).

were prepared. The centrifugation procedure led to the following order of decreasing particle weight in the suspension: B > C > D, whereas suspension A contains all possible particle dimensions. The different suspensions are stable from a few hours to several weeks and any of the suspensions can be easily redispersed by simple stirring, which enables long-term use of the colloids.

Fig. 1c shows the Raman spectrum of suspension D measured with an excitation wavelength of 532 nm and an optical power of 2 mW. Raman spectra of all four colloids present similar features (Fig. S2–S4, ESI†), indicating that LPE results in analogous structures. The Raman spectra are in agreement with those of the bulk[30–33] and with those of mechanically exfoliated few-layer TiS_3,[34] with additional bands that indicate the presence of TiO_2 in the form of the anatase polytype,[35,36] probably due to surface/edge oxidation of TiS_3. Raman analysis of the bulk confirms that TiO_2 is found right from the beginning in the starting material, but further oxidation during the sonication process cannot be excluded.[37]

The optical properties of liquid-phase-exfoliated TiS_3 were studied by UV–Vis–NIR spectroscopy (Fig. 1d and Fig. S5, ESI†). These absorption properties are in agreement with an optical bandgap of 1.07 eV (corresponding to an absorption onset of 1160 nm) reported for as synthesized bulk material.[38] This is expected as the band structure of TiS_3 is mostly thickness independent.[38,39] The Tauc plot (Fig. S6, ESI†), which is generated from the absorption data of suspension D, confirms that the TiS_3 nanoribbons have a direct optical bandgap of 1.02 eV, consistent with values from the literature.[29,38,40]

In order to integrate liquid-phase-exfoliated TiS_3 into functional devices, we employed DEP-assisted deposition. In the DEP phenomenon, a non-uniform electric field polarizes the suspended particles of a colloid within the corresponding solvent and gradients in the electric field force the alignment of the particles (dipoles) with the local field lines and push these particles towards regions of most intense field. The relative polarizabilities of both components of the colloid (suspended particles and solvent) are crucial for this process. In previous studies, DEP has been used successfully as a method to assemble carbon nanotubes[41] or graphene[42–44] between metallic electrodes, but its use with other two-dimensional materials is rather scarce and very recent.[28]

In our implementation of the technique, sketched in Fig. 2a, a 1 MHz sinusoidal signal of 10 V peak-to-peak is applied between drain and source electrodes, which are separated by 5 μm. A drop of the TiS_3 colloidal suspension is cast onto the electrodes and the electric field generated by the oscillating source–drain voltage polarizes the nanoribbons with respect to the solvent. The gradients in the electric fields push these nanoribbons toward the region of highest electric field intensity. TiS_3 nanoribbons are thus deposited in a controlled way, preferentially bridging the electrodes, between which the electric field intensity is the highest. This allows the fabrication of a fully packed TiS_3 channel out of a suspension of relatively low concentration. TiS_3 LPE was performed in IPA due to its ability to efficiently stabilize the resulting colloidal nanoribbons, its relatively low boiling point, and its weak polarizability (≈7 Å^3, see ref. 45). The DEP force acting on tube-shaped particles (which is a good approximation to the TiS_3 nanoribbons) can be written as:

$$F_{\mathrm{DEP}} \propto \varepsilon_{\mathrm{m}}\,\mathrm{Re}[(\varepsilon_{\mathrm{p}}^{*} - \varepsilon_{\mathrm{m}}^{*})/(\varepsilon_{\mathrm{m}}^{*})]\nabla|E|^{2}$$

where $\varepsilon_{\mathrm{p}}^{*}$ and $\varepsilon_{\mathrm{m}}^{*}$ are the complex permittivities of the particles and the suspension medium, respectively, and E is the electric field. If a suspended particle has a polarizability higher than that of the medium, $|\varepsilon_{\mathrm{p}}^{*}| > |\varepsilon_{\mathrm{m}}^{*}|$, the force will push the particle into the regions where the electric field intensity is the highest.

From now on in the main text we will focus on the DEP-based assembly from suspension D, which contains the smallest particles. A SEM image of the resulting device is shown in Fig. 2b and c shows a zoom in the region separating one particular pair of electrodes. From these images, it can be seen that most of the TiS_3 nanoribbons have accumulated in the region between

the electrodes, where the source and drain electrodes face each other, with only a small amount of the material deposited on the side of the electrodes or on the SiO_2 surface. Moreover, thanks to DEP-assisted deposition, TiS_3 nanoribbons mostly adopt an orientation that is parallel to the source–drain direction, as confirmed by the analysis of the angular distribution of the nanoribbons in relation to the electrodes shown in Fig. 2d. The peak at 0° indicates that the preferred TiS_3 configurations are those in which the nanoribbon length is parallel to the source–drain direction (Fig. S7, ESI†). A distribution of the nanoribbon lengths is shown in Fig. S8 of the ESI.†

After the DEP assembly, we characterized the electrical transport of the fabricated device at room temperature and under high-vacuum conditions ($P \approx 2 \times 10^{-6}$ mbar). Fig. 3a shows the current–voltage (I–V) characteristics of the device recorded in the dark and under illumination with a blue laser (λ = 405 nm). The laser has been focused on the device surface in a spot size of approximately 120 μm diameter. Under dark conditions, the I–V characteristic is asymmetric in bias and the maximum current flowing through the device reaches approximately 25 μA at a bias voltage of 1 V. Upon illumination, the device shows an enhancement of the current because of the photogeneration of charge carriers, visible in the I–V curves of Fig. 3a recorded for increasing laser intensities. For samples with a large amount of loosely connected nanoribbons the electrical characteristics turned out not to be reproducible because of continuous switching that we attribute to the electromechanical motion of the nanoribbons. See for example a device built from suspension A (Fig. S9 and S10, ESI†) which shows frequent switches in current with and without illumination.

The generated photocurrent in the device made from suspension D reaches a value of 7.4 μA at 1 V with a light/dark current ratio of 1.3. Fig. 3b shows the responsivity of the device at a bias of 1 V as a function of the incident laser power P_D. The responsivity at each laser power is calculated from the I–V curves by dividing the photocurrent at a voltage of 1 V by the product of the total incident illumination power density and the active area of the device. The largest responsivity is 3.8 mA W^{-1}, recorded for the largest excitation power P_D. The extracted responsivity is low when compared to that of a single TiS_3 nanoribbon[26] which is many orders of magnitude higher. This can be explained by the fact that in the present case the transport in the device is dominated by the TiS_3/TiS_3 interfaces and not by the intrinsic TiS_3 material properties, giving lower overall performances, as was already observed[18] in the case of LPE MoS_2. Interestingly, the responsivity shows a pronounced linear dependence on the excitation power. This monotonous increase in responsivity for increasing incident power is relatively unusual in low-dimensional semiconducting photodetectors, for which a monotonous decrease as a function of power is usually observed. Such a linear increasing behavior has been explained theoretically in other semiconducting devices by the presence of recombination centers with different intragap energies in the semiconductor.[18,46] The incident light shifts the Fermi level, thus changing the occupancy of these centers, which can result in a larger lifetime of the carriers at higher incident power densities. Due to the LPE method our devices are likely to contain various defects, which could account for the linear dependence of the responsivity on the excitation power.

Finally, in order to study the time response of the device we measured the source–drain current as a function of time while switching on and off the illumination. Fig. 3c shows the photocurrent recorded during several switching cycles at a bias voltage of 10 mV and with increasing illumination power. The response time extracted from Fig. 3d is $\tau = (8 \pm 2)$ s. In addition, we studied the photoresponse with a laser of 638 nm in order to rule out a possible contribution to the photoresponse due to the presence of TiO_2 given its negligible response for excitation wavelengths longer than 500 nm.[47] The small variations in the responsivity at 638 nm and 405 nm (Fig. S11, ESI†) are in good agreement with the energy dependence of TiS_3 nanoribbon absorptivity, excluding any significant contribution of TiO_2 to the photoresponse of the device.

In conclusion, we have studied a solid-state photodetector based on liquid-phase-exfoliated TiS_3 nanoribbons. We have shown that a dielectrophoresis-based deposition method can produce high-quality devices by assembling the TiS_3 ink onto metallic electrodes. Electrical and optical measurements reveal that the responsivities and the general performances of our devices are better compared to state-of-the-art photodetectors based on liquid-phase-exfoliated materials.

We acknowledge funding from the European Commission (Graphene Flagship, CNECTICT-604391). A. C. G. acknowledges

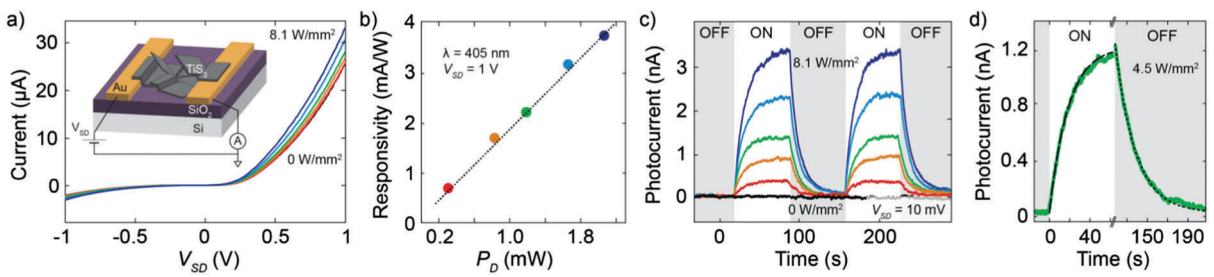

Fig. 3 (a) Current–voltage characteristics of the LPE-based TiS_3 device in the dark and upon illumination with a laser (wavelength 405 nm) for increasing light power densities up to 8.1 W mm^{-2}. Inset: Schematic illustration of the fabricated device. (b) Responsivity at a bias voltage of 1 V as a function of light power. The dashed line is a linear fit to the data. (c) Time response of the photocurrent recorded at a bias voltage of 10 mV upon a modulated optical excitation (frequency 8 mHz) for increasing laser power densities up to 8.1 W mm^{-2}. (d) Time response at an optical power density of 4.5 W mm^{-2}. The dashed lines are fit to an exponential decay function; the time constant of the system is 8 ± 2 s.

financial support from the MINECO (Ramón y Cajal 2014 RYC-2014-01406 and MAT2014-58399-JIN) and from the Comunidad de Madrid (MAD2D-CM Program (S2013/MIT-3007)). R. F. acknowledges support from NWO through the research program Rubicon with project number 680-50-1515. D. PdL. acknowledges the support from MICINN/MINECO (Spain) through the program FIS2015-67367-C2-1-P. E. M. P. acknowledges funding from the European Research Council MINT (ERC-StG-2012-307609), the MINECO of Spain (CTQ2014-60541-P) and the Comunidad de Madrid (MAD2D project, S2013/MIT-3007). E. G. acknowledges support from the AMAROUT II program (Marie Curie Action, FP7-PEOPLE-2011-COFUND (291803)). E. F., C. S., J. R. A. and I. J. Ferrer acknowledge support from MINECO through the project MAT2015-65203R.

Notes and references

1 K. S. Novoselov, A. K. Geim, S. V. Morozov, D. Jiang, Y. Zhang, S. V. Dubonos, I. V. Grigorieva and A. A. Firsov, *Science*, 2004, **306**, 666–669.
2 M. Yi and Z. Shen, *J. Mater. Chem. A*, 2015, **3**, 11700–11715.
3 A. Castellanos-Gomez, M. Buscema, R. Molenaar, V. Singh, L. Janssen, H. S. van der Zant and G. A. Steele, *2D Mater.*, 2014, **1**, 011002.
4 Y. H. Lee, X. Q. Zhang, W. Zhang, M. T. Chang, C. T. Lin, K. D. Chang, Y. C. Yu, J. T. W. Wang, C. S. Chang and L. J. Li, *Adv. Mater.*, 2012, **24**, 2320–2325.
5 Y. Zhan, Z. Liu, S. Najmaei, P. M. Ajayan and J. Lou, *Small*, 2012, **8**, 966–971.
6 H. Schmidt, S. Wang, L. Chu, M. Toh, R. Kumar, W. Zhao, A. Castro Neto, J. Martin, S. Adam and B. Özyilmaz, *Nano Lett.*, 2014, **14**, 1909–1913.
7 Y. Hernandez, V. Nicolosi, M. Lotya, F. M. Blighe, Z. Sun, S. De, I. McGovern, B. Holland, M. Byrne and Y. K. Gun'Ko, *Nat. Nanotechnol.*, 2008, **3**, 563–568.
8 J. N. Coleman, *Adv. Funct. Mater.*, 2009, **19**, 3680–3695.
9 J. N. Coleman, M. Lotya, A. O'Neill, S. D. Bergin, P. J. King, U. Khan, K. Young, A. Gaucher, S. De and R. J. Smith, *Science*, 2011, **331**, 568–571.
10 V. Nicolosi, M. Chhowalla, M. G. Kanatzidis, M. S. Strano and J. N. Coleman, *Science*, 2013, **340**, 1226419.
11 A. Ciesielski and P. Samorì, *Chem. Soc. Rev.*, 2014, **43**, 381–398.
12 L. Niu, J. N. Coleman, H. Zhang, H. Shin, M. Chhowalla and Z. Zheng, *Small*, 2016, **12**, 272–293.
13 D. Fadil, R. H. Fayaz and A. B. Kaul, *MRS Adv.*, 2016, **1**, 3223–3228.
14 A. B. Bourlinos, V. Georgakilas, R. Zboril, T. A. Steriotis and A. K. Stubos, *Small*, 2009, **5**, 1841–1845.
15 G. S. Bang, K. W. Nam, J. Y. Kim, J. Shin, J. W. Choi and S.-Y. Choi, *ACS Appl. Mater. Interfaces*, 2014, **6**, 7084–7089.
16 P. Yasaei, B. Kumar, T. Foroozan, C. Wang, M. Asadi, D. Tuschel, J. E. Indacochea, R. F. Klie and A. Salehi-Khojin, *Adv. Mater.*, 2015, **27**, 1887–1892.
17 A. G. Kelly, T. Hallam, C. Backes, A. Harvey, A. S. Esmaeily, I. Godwin, J. Coelho, V. Nicolosi, J. Lauth, A. Kulkarni, S. Kinge, L. D. A. Siebbeles, G. S. Duesberg and J. N. Coleman, *Science*, 2017, **356**, 69–73.
18 S. Ghosh, A. Winchester, B. Muchharla, M. Wasala, S. Feng, A. L. Elias, M. B. M. Krishna, T. Harada, C. Chin, K. Dani, S. Kar, M. Terrones and S. Talapatra, *Sci. Rep.*, 2015, **5**, 11272.
19 K. Lee, H.-Y. Kim, M. Lotya, J. N. Coleman, G.-T. Kim and G. S. Duesberg, *Adv. Mater.*, 2011, **23**, 4178–4182.
20 F. Torrisi, T. Hasan, W. Wu, Z. Sun, A. Lombardo, T. S. Kulmala, G.-W. Hsieh, S. Jung, F. Bonaccorso and P. J. Paul, *ACS Nano*, 2012, **6**, 2992–3006.
21 D. L. Gonzalez Arellano, H. Lee, E. B. Secor, E. K. Burnett, M. C. Hersam, J. J. Watkins and A. L. Briseno, *ACS Appl. Mater. Interfaces*, 2016, **8**, 29594–29599.
22 F. Withers, H. Yang, L. Britnell, A. P. Rooney, E. Lewis, A. Felten, C. R. Woods, V. Sanchez Romaguera, T. Georgiou, A. Eckmann, Y. J. Kim, S. G. Yeates, S. J. Haigh, A. K. Geim, K. S. Novoselov and C. Casiraghi, *Nano Lett.*, 2014, **14**, 3987–3992.
23 H. Yang, F. Withers, E. Gebremedhn, E. Lewis, L. Britnell, A. Felten, V. Palermo, S. Haigh, D. Beljonne and C. Casiraghi, *2D Mater.*, 2014, **1**, 011012.
24 J. Zhu, J. Kang, J. Kang, D. Jariwala, J. D. Wood, J.-W. T. Seo, K.-S. Chen, T. J. Marks and M. C. Hersam, *Nano Lett.*, 2015, **15**, 7029–7036.
25 J. O. Island, R. Biele, M. Barawi, J. M. Clamagirand, J. R. Ares, C. Sánchez, H. S. van der Zant, I. J. Ferrer, R. D'Agosta and A. Castellanos-Gomez, *Sci. Rep.*, 2016, **6**.
26 J. O. Island, M. Buscema, M. Barawi, J. M. Clamagirand, J. R. Ares, C. Sánchez, I. J. Ferrer, G. A. Steele, H. S. van der Zant and A. Castellanos-Gomez, *Adv. Opt. Mater.*, 2014, **2**, 641–645.
27 J. O. Island, M. Barawi, R. Biele, A. Almazan, J. M. Clamagirand, J. R. Ares, C. Sanchez, H. S. van der Zant, J. V. Alvarez, R. D'Agosta, I. J. Ferrer and A. Castellanos-Gomez, *Adv. Mater.*, 2015, **27**, 2595–2601.
28 D. D. Deng, Z. Lin, A. L. Elías, N. Perea-Lopez, J. Li, C. Zhou, K. Zhang, S. Feng, H. Terrones and J. S. Mayer, *ACS Nano*, 2016, **10**, 5006–5014.
29 I. J. Ferrer, M. D. Maciá, V. Carcelén, J. R. Ares and C. Sánchez, *Energy Procedia*, 2012, **22**, 48–52.
30 S. P. Gwet, Y. Mathey and C. Sourisseau, *Phys. Status Solidi B*, 1984, **123**, 503–517.
31 D. W. Bullett, in *Theoretical aspects of band structures and electronic properties of pseudo-one-dimensional solids*, ed. H. Kamimura and D. Reidel Publishing Company, Dordrecht, Holland, 1985, pp. 160–230.
32 P. Gard, F. Cruege, C. Sourisseau and O. Gorochov, *J. Raman Spectrosc.*, 1986, **17**, 283–288.
33 A. S. Pawbake, J. O. Island, E. Flores, J. R. Ares, C. Sanchez, I. J. Ferrer, S. R. Jadkar, H. S. J. van der Zant, A. Castellanos-Gomez and D. J. Late, *ACS Appl. Mater. Interfaces*, 2015, **7**, 24185–24190.
34 A. Lipatov, P. M. Wilson, M. Shekhirev, J. D. Teeter, R. Netusil and A. Sinitskii, *Nanoscale*, 2015, **7**, 12291–12296.
35 T. Ohsaka, F. Izumi and Y. Fujiki, *J. Raman Spectrosc.*, 1978, **7**, 321–324.
36 L. Mahoney and R. Koodali, *Materials*, 2014, **7**, 2697–2746.
37 A. Jawaid, D. Nepal, K. Park, M. Jespersen, A. Qualley, P. Mirau, L. F. Drummy and R. A. Vaia, *Chem. Mater.*, 2016, **28**, 337–348.
38 A. J. Molina-Mendoza, M. Barawi, R. Biele, E. Flores, J. R. Ares, C. Sánchez, G. Rubio-Bollinger, N. Agraït, R. D'Agosta, I. J. Ferrer and A. Castellanos-Gomez, *Adv. Electron. Mater.*, 2015, **1**, 1500126.
39 J. Dai and X. C. Zeng, *Angew. Chem., Int. Ed.*, 2015, **54**, 7572–7576.
40 J. O. Island, M. Barawi, R. Biele, A. Almazán, J. M. Clamagirand, J. R. Ares, C. Sánchez, H. S. J. van der Zant, J. V. Álvarez, R. D'Agosta, I. J. Ferrer and A. Castellanos-Gomez, *Adv. Mater.*, 2015, **27**, 2595–2601.
41 A. Vijayaraghavan, S. Blatt, D. Weissenberger, M. Oron-Carl, F. Hennrich, D. Gerthsen, H. Hahn and R. Krupke, *Nano Lett.*, 2007, **7**, 1556–1560.
42 C. D. Sire, F. Ardiaca, S. Lepilliet, J.-W. T. Seo, M. C. Hersam, G. Dambrine, H. Happy and V. Derycke, *Nano Lett.*, 2012, **12**, 1184–1188.
43 B. R. Burg, J. Schneider, S. Maurer, N. C. Schirmer and D. Poulikakos, *J. Appl. Phys.*, 2010, **107**, 034302.
44 B. R. Burg, F. Lütolf, J. Schneider, N. C. Schirmer, T. Schwamb and D. Poulikakos, *Appl. Phys. Lett.*, 2009, **94**, 053110.
45 R. Bosque and J. Sales, *J. Chem. Inf. Comput. Sci.*, 2002, **42**, 1154–1163.
46 V. Klee, E. Preciado, D. Barroso, A. E. Nguyen, C. Lee, K. J. Erickson, M. Triplett, B. Davis, I.-H. Lu and S. Bobek, *Nano Lett.*, 2015, **15**, 2612–2619.
47 A. Molina-Mendoza, A. Moya, R. Frisenda, S. A. Svatek, P. Gant, S. Gonzalez-Abad, E. Antolín, N. Agrait, G. R. Bollinger and D. P. de Lara, *J. Mater. Chem. C*, 2016, **4**, 10707–10714.